DOI: 10.1002/ejic.201200274

Trimetallic $[M_3(dpa)_4]^{2+}$ Complexes (M = Co, Ni) as Building Blocks for Cyano-Bridged Coordination Polymers

Jingfang Wang,[a,b] Andrew Ozarowski,[b] Kirill Kovnir,[a][‡] Corey M. Thompson,[a] Alexander A. Yaroslavtsev,[c] Roman V. Chernikov,[d] Naresh S. Dalal,*[a,b] and Michael Shatruk*[a,b]

Keywords: Coordination polymers / Cyanides / Magnetic properties / Spin crossover / Charge transfer

Reactions between the complexes $M_3(dpa)_4Cl_2$ (M = Co, Ni; dpa = 2,2′-dipyridylamine), which contain linear trimetallic fragments, and $(Bu_4N)_3[M'(CN)_6]$ (M′ = Fe, Co) result in the formation of CN-bridged coordination polymers. The analysis of the products obtained suggests that they have a two-dimensional structure, in which ditopic $[M_3(dpa)_4]^{2+}$ linkers bridge 4-connected $[M'(CN)_6]^{3-}$ nodes into an extended layer. The synthesis of $\{[Co_3(dpa)_4]_{1.97}[Fe(CN)_6]\}Cl_{0.8}$ (**1**) is accompanied by an electron transfer from the tricobalt to the hexacyanoferrate units, which results in the formation of $[Co_3(dpa)_4]^{3+}$ and $[Fe(CN)_6]^{4-}$ fragments. In $\{[Ni_3(dpa)_4]_{1.74}[Fe(CN)_6]\}Cl_{0.45}$ (**3**), a partial charge transfer between the trinickel and the hexacyanoferrate units leads to the temperature-dependent Fe^{III}/Fe^{II} mixed valence, and lower temperatures favor the thermodynamic Fe^{III} ground state. $\{[Co_3(dpa)_4]_{2.06}[Co(CN)_6]\}Cl_{1.1}$ (**2**) exhibits spin-glass behavior with a spin-freezing point of approximately 4.8 K, which is due to the magnetic superexchange between the paramagnetic $[Co_3(dpa)_4]^{2+}$ (S = 1/2) units through the diamagnetic $[Co(CN)_6]^{3-}$ linkers.

Introduction

Despite the tercentennial history of Prussian blue (PB), considered by many as the first molecule-based coordination compound, this solid and its analogues continue to be the focus of extensive research. Over the last two decades, the PB-type compounds have been shown to exhibit fascinating properties, such as high-temperature magnetism,[1–3] photomagnetism,[4,5] hydrogen-gas uptake,[6,7] and negative thermal expansion.[8–10] Recent efforts in the synthesis of new derivatives of PB have been developing along two main directions. The first one employs blocking ligands that "cut out" extended or finite fragments from the 3D structure of PB.[11] In this manner, a large number of unique low-dimensional structures have been prepared, especially for the study of single-chain magnets[12–14] and single-molecule magnets.[15–20] The other direction focuses on expanding the building blocks that constitute the PB structure. Thus, metal–metal-bonded dimers[21–24] or octahedral metal clusters[25–27] have been substituted for single metal ions, which either preserved the PB topology or resulted in new structural motifs.

Our interest in designing new coordination compounds derived from PB has led us to explore trimetallic clusters $M_3(dpa)_4X_2$ (M = Cr, Co, Ni, Ru; dpa^- = 2,2′-dipyridylamine; X^- = Cl^-, CN^-, BF_4^-), which were studied in detail by the groups of Peng and Cotton.[28–35] These unique molecules have been largely overlooked as possible building blocks for larger molecule-based structures. The two sites occupied by axial ligands X (Scheme 1) offer convenient points for the structural expansion. Moreover, the trimetallic clusters themselves exhibit interesting electronic and magnetic properties; $Co_3(dpa)_4Cl_2$ and $Ni_3(dpa)_4Cl_2$ exhibit gradual temperature-induced spin crossover.[31,36,37]

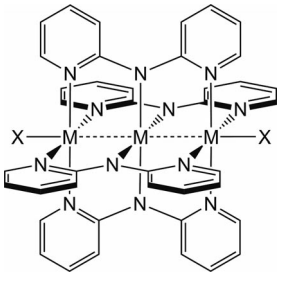

Scheme 1. Molecular structure of $M_3(dpa)_4X_2$ clusters.

[a] Department of Chemistry and Biochemistry, Florida State University,
95 Chieftan Way, Tallahassee, FL 32306, USA
Fax: +1-850-644-8281
E-mail: shatruk@chem.fsu.edu
[b] National High Magnetic Field Laboratory, Florida State University,
800 E Paul Dirac Dr, Tallahassee, FL 32310, USA
[c] National Research Nuclear University "MEPhI",
115409 Moscow, Russia
[d] HASYLAB at DESY,
22603 Hamburg, Germany
[‡] Present address: Department of Chemistry, University of California at Davis,
Davis, CA 95616, USA

Supporting information for this article is available on the WWW under http://dx.doi.org/10.1002/ejic.201200274.

To this date, only a few structures built by extension of the trimetallic clusters have been reported,[38] all of them with the $[Ni_3(dpa)_4]^{2+}$ building block. The trimetallic units were connected by mono- or dianionic μ_2-bridging ligands into chain compounds, $[Ni_3(dpa)_4(\mu\text{-}L)](X)$ [L and X = $(MeO)C_4O_3^-$ and BF_4^- or N_3^- and PF_6^-][39] and $[Ni_3(dpa)_4(\mu\text{-}L)]$ (L = phthalate or 3-nitrophthalate).[40] The use of $[Ni_3(dpa)_4]^{2+}$ in conjunction with another metal-containing building block produced either chain structures, $\{[Ni_3(dpa)_4][(TPP)Mn(L)]\}(ClO_4)$ [TPP = tetraphenylporphyrinate, L = 3- or 4-pyridinecarboxylate (4-pyCO_2^-)],[41] or finite complexes, $\{[Ni_3(dpa)_4][(TPP)Zn(4\text{-}pyCO_2)]_2\}$[41] and $\{[Ni_3(dpa)_4][Ag(CN)_2]_2\}$.[42] The latter is the only known structure based on the $[M_3(dpa)_4]^{2+}$ building blocks that utilizes CN^- as a bridging ligand.

Inspired by the aforementioned examples of PB-like structures based on expanded building blocks, we have decided to substitute the trimetallic $[M_3(dpa)_4]^{2+}$ units for the single metal ions in the PB structure. Herein, we report findings from our initial efforts in this direction, including the synthesis of CN-bridged coordination polymers with trinickel and tricobalt clusters, their possible structures and magnetic behavior, and unprecedented temperature-dependent charge transfer involving trimetallic units.

Results and Discussion

Synthesis

It is known that the preparation of the trinickel complex $Ni_3(dpa)_4Cl_2$ requires the use of rigorously dehydrated $NiCl_2$.[31] Berry et al. demonstrated that the synthesis could be simplified by using an $Ni(Hdpa)_2Cl_2$ precursor, deprotonation of which with methyllithium afforded the desired trinuclear complex.[43] In this process, however, 1/3 of Hdpa molecules were not included in the final product. We have found that $Ni(Hdpa)Cl_2$[44] can be used as an alternative precursor. A reaction between $Ni(Hdpa)Cl_2$ and free Hdpa in a 3:1 molar ratio in the presence of CH_3Li produces crystalline $Ni_3(dpa)_4Cl_2{\cdot}1.2CH_2Cl_2$ in 85% yield. In addition to the improved yield, no Hdpa ligand is wasted in the course of the reaction. The tricobalt cluster was synthesized according to the reported method.[45]

Reactions of the trinuclear complexes $M_3(dpa)_4Cl_2$ (M = Co, Ni) with hexacyanometalates $(Bu_4N)_3[M'(CN)_6]$ (M′ = Fe, Co) in DMF result in precipitation of highly insoluble products. The precipitate forms over the course of several minutes in the case of M = Co and of several hours in the case of M = Ni. The color of the final products, the wavelength at the absorption maximum in the visible range (Figure S1), and the M/M′/Cl ratio established by an energy-dispersive X-ray (EDX) microanalysis are given in Table 1. The obtained elemental analysis data allow us to formulate a general composition of these materials as $\{[M_3(dpa)_4]_{2-x}[M'(CN)_6]\}Cl_y$. The derived compositions are in good agreement with the results of conventional (C,H,Cl,N) elemental analyses (see the Experimental Section).

Proposed Structure

The insolubility of the compounds **1**–**4** in all common solvents suggests that their structures correspond to CN-bridged coordination polymers, which is similar to the formation of insoluble products of the PB family.[46] The building blocks used in the synthesis, $[M_3(dpa)_4]^{2+}$ and $[M'(CN)_6]^{3-}$, can be considered as a ditopic linker and a six-connected node, respectively, using the common terminology for metal–organic frameworks. The most obvious way to combine these units in a CN-bridged structure is to form a 3D framework $\{[\mu_2\text{-}M_3(dpa)_4]_3[M'(CN)_6]\}Cl_3$, but the M/M′ ratio (9:1) in such a framework is much higher than the ratios found in **1**–**4** (Table 1). Therefore, the connectedness of the $[M'(CN)_6]^{3-}$ nodes should be decreased to conform to the determined composition. The most likely structure to give an M/M′ ratio of approximately 6:1 is the one in which $[M'(CN)_6]^{3-}$ ions act as four-connected nodes bound through the ditopic $[M_3(dpa)_4]^{2+}$ linkers into a two-dimensional coordination polymer (Scheme 2). The ideal composition of such a layered structure is $\{[\mu_2\text{-}M_3(dpa)_4]_2[M'(CN)_6]\}Cl$, which is close to the ones found experimentally.

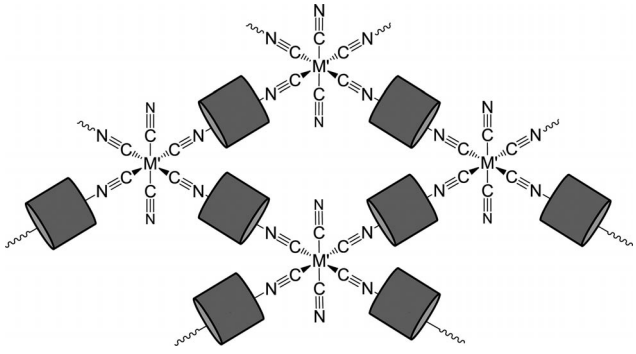

Scheme 2. Proposed layered structure of compounds **1**–**4**. The trimetallic $[M_3(dpa)_4]^{2+}$ units (M = Co, Ni) are represented by grey cylinders.

Table 1. Elemental analysis of compounds **1**–**4**.

M/M′	Color (λ_{max} vis[a])	M/M′/Cl atomic ratio (EDX)[b]	Proposed composition
Co/Fe (**1**)	dark brown (567 nm)	5.9:1.0:0.8	$\{[Co_3(dpa)_4]_{1.97}[Fe(CN)_6]\}Cl_{0.8}$
Co/Co (**2**)	dark brown (613 nm)	6.4:1.0[c]	$\{[Co_3(dpa)_4]_{2.06}[Co(CN)_6]\}Cl_{1.1}$
Ni/Fe (**3**)	dark purple (595 nm)	5.2:1.0:0.45	$\{[Ni_3(dpa)_4]_{1.74}[Fe(CN)_6]\}Cl_{0.45}$
Ni/Co (**4**)	dark purple (636 nm)	4.7:1.0:0.3	$\{[Ni_3(dpa)_4]_{1.57}[Co(CN)_6]\}Cl_{0.3}$

[a] λ_{max} in the visible region. [b] The uncertainty of the EDX elemental analysis is < 0.1. The proposed compositions are charge-balanced within this uncertainty. [c] The (M + M′)/Cl atomic ratio is given for **2**, because M = M′.

Another possibility is the formation of a one-dimensional coordination polymer, in which each $[M'(CN)_6]^{3-}$ node is connected to only two $[M_3(dpa)_4]^{2+}$ linkers, but in such a structure the M/M′ ratio is 3:1, which is much lower than the ratios determined experimentally.

The foregoing considerations suggest that the products **1**–**4** are likely to have layered 2D structures, in which each $[M(CN)_6]^{3-}$ unit uses four of its CN^- ligands to connect to $[M_3(dpa)_4]^{2+}$ units, whereas the other two CN^- ligands remain terminal. The formation of the proposed 2D structure instead of the anticipated PB-like 3D framework can be justified by taking into account the bulky organic sheath of four dpa^- ligands that surround the trimetallic unit (Scheme 1). It is likely that six sterically demanding $[M_3(dpa)_4]^{2+}$ units cannot fit around the central $[Fe(CN)_6]^{3-}$ ion to afford the 3D CN-bridged polymer. On the other hand, in the 2D structure, such steric limitations can be avoided through buckling of the layers. The experimentally observed decrease from the ideal M/M′ ratio of 6:1 can be explained by the formation of vacancies in the positions of $[M_3(dpa)_4]^{2+}$ fragments, which appears to correlate with the content of Cl^- counterions (Table 1) to maintain the overall charge balance. This is not surprising, as a similar situation is observed for PB-type structures, $A_xM[M'(CN)_6]_y$ (A = alkali metal), in which the concentration of $[M'(CN)_6]^{n-}$ vacancies correlates with the concentration of the A^+ counterions.[47,48] A significant disorder is quite common for such insoluble, quickly precipitating products, as indicated by the broad distribution of observed compositions for the products **1**–**4** as well as by their amorphousness, which is evident from the lack of discernible powder X-ray diffraction patterns.

Mössbauer Spectroscopy

Mössbauer spectra of the Fe-containing complexes **1** and **3** were collected at 5 and 295 K (Table 2). At both temperatures, the spectrum of **1** (Figure 1a) is dominated by a singlet with low isomer shift (δ), which is characteristic of low-spin (LS) Fe^{II} ions. A much weaker signal with low δ and large quadrupole splitting (ΔE_Q) is assigned to LS Fe^{III} ions. In contrast, the 295 K spectrum of **3** (Figure 1b) reveals the presence of LS Fe^{II} and LS Fe^{III} ions in comparable amounts (Fe^{II}/Fe^{III} = 45:55). Moreover, this ratio is temperature-dependent, as the relative amount of LS Fe^{III} ions significantly increases at 5 K (Fe^{II}/Fe^{III} = 21:79). When the sample is warmed up to 295 K again, the original Fe^{II}/Fe^{III} ratio of 45:55 is fully recovered, which points to the reversibility of the charge-transfer process.

Table 2. Parameters of Mössbauer spectra of compounds **1** and **3**.

Complex	T [K]	Fe type	δ [mm s^{-1}]	ΔE_Q [mm s^{-1}]	Relative content
1	295	LS Fe^{II}	–0.07		89%
		LS Fe^{III}	–0.13	1.25	11%
	5	LS Fe^{II}	0.00		85%
		LS Fe^{III}	–0.05	1.76	15%
3	295	LS Fe^{II}	–0.04		45%
		LS Fe^{III}	–0.16	1.32	55%
	5	LS Fe^{II}	0.02		29%
		LS Fe^{III}	0.05	1.81	71%

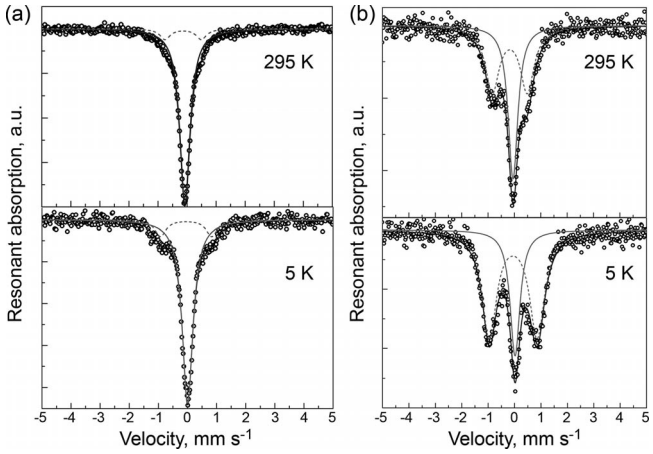

Figure 1. Mössbauer spectra of **1** (a) and **3** (b). The solid and dashed grey lines are simulated contributions of LS Fe^{II} and LS Fe^{III} ions, respectively. The solid black line represents the sum of the contributions of all types of Fe ions in the sample.

Infrared Spectroscopy

Terminal cyano ligands of $(Bu_4N)_3[Fe(CN)_6]$ and $(Bu_4N)_3[Co(CN)_6]$ exhibit sharp C≡N stretching bands at 2096 cm^{-1} and 2106 cm^{-1}, respectively. For bridging CN^- ligands, the C≡N stretching bands usually shift to higher frequencies, as a result of the depletion of electron density in the weakly antibonding 5σ orbital of the CN^- ligand.[11] Indeed, the IR spectra of **2** and **4**, both of which contain hexacyanocobaltate fragments, show bands at slightly higher energies than that observed for $(Bu_4N)_3[Co(CN)_6]$ (Figure 2 and Table 3). In striking contrast, the IR spectra of **1** and **3** exhibit pronounced C≡N stretching bands at significantly lower frequencies than those of $(Bu_4N)_3[Fe(CN)_6]$. Noteworthy, the bands observed for the hexacyanometalate precursors in the range 2800–3000 cm^{-1}, attributed to characteristic vibrations of Bu_4N^+ cations (Figure 2, bottom), are absent in the spectra of **1**–**4**, which thus confirms that these cations are not included in the final products (Table 1).

These observations support the findings obtained with Mössbauer spectroscopy, because they provide a strong indication for the presence of Fe^{II} centers in the products **1** and **3**. Only such a scenario can justify the significant decrease in the C≡N stretching frequency, which results from the increased π back-bonding from the Fe^{II} ions. A similar situation is observed when the classical PB is prepared by a reaction between aqueous solutions of Fe^{II} and $[Fe^{III}(CN)_6]^{3-}$ ions. Because of instantaneous electron transfer, the final product is formulated as $Fe^{III}_4[Fe^{II}(CN)_6]_3 \cdot 14H_2O$. It contains Fe^{II} ions in the environment of *C*-bound bridging CN^- ligands with $\tilde{\nu}_{CN}$ = 2080 cm^{-1}.[51] This value, compared to $\tilde{\nu}_{CN}$ of the free $[Fe^{II}(CN)_6]^{4-}$ ion (2040 cm^{-1}), appears at higher energy, as expected for bridging cyanides.

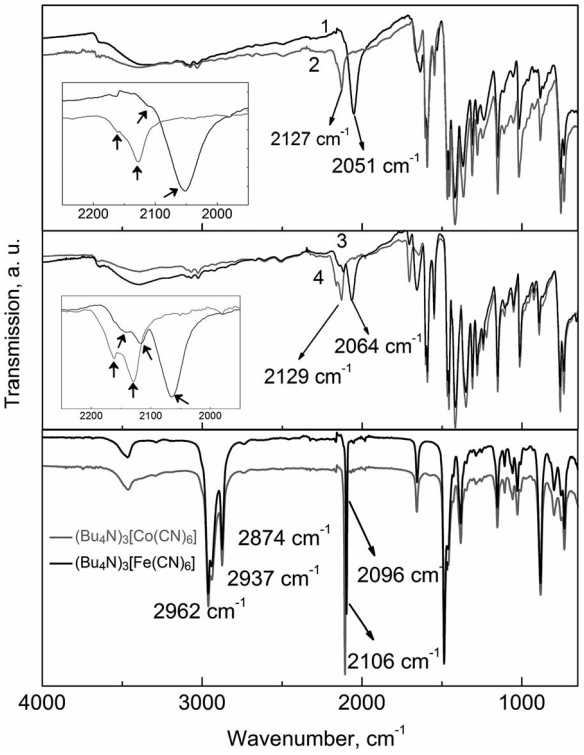

Figure 2. Infrared spectra of products **1** and **2** (top), **3** and **4** (middle), and the starting materials $(Bu_4N)_3[M'(CN)_6]$, M′ = Fe, Co (bottom). Insets: magnified region of C≡N stretching bands; the arrows indicate specific features discussed in the text and summarized in Table 3.

Table 3. C≡N stretching bands and their assignments[a] in the IR spectra of compounds **1**–**4** and of some reference complexes.

Compound	$\tilde{\nu}_{CN}$ [cm^{-1}]	Comment
1	2051 (ter), 2110 (br)	Fe^{II}
2	2127 (ter), 2160 (br)	Co^{III}
3	2064 (ter), 2116 (br)	Fe^{II}
	2116 (ter), 2146 (br)	Fe^{III}
4	2129 (ter), 2162 (br)	Co^{III}
$K_4[Fe^{II}(CN)_6]$	2040 (ter)	ref.[11]
$K_2Co^{II}[Fe^{II}(CN)_6]$	2080 (br)	ref.[49]
$(Bu_4N)_3[Fe^{III}(CN)_6]$	2096 (ter)	this work
$Ni^{II}_3[Fe^{III}(CN)_6]_2$	2166 (br)	ref.[50]
$(Bu_4N)_3[Co^{III}(CN)_6]$	2106 (ter)	this work
$Co^{II}_3[Co^{III}(CN)_6]_2$	2170 (br)	ref.[50]
$Ni^{II}_3[Co^{III}(CN)_6]_2$	2176 (br)	ref.[50]

[a] ter = terminal; br = bridging.

Besides the aforementioned intense bands, weaker signals are also observed in the region characteristic of C≡N stretching bands for **1**–**4** (Figure 2, insets). These bands are summarized in Table 3 along with the $\tilde{\nu}_{CN}$ values of some reference compounds. By correlating the obtained IR spectra to the proposed structure of **1**–**4** (Scheme 2), we assign the intense C≡N stretching bands observed in **2** (2127 cm^{-1}) and **4** (2129 cm^{-1}) to the terminal CN^- ligands of $[Co^{III}(CN)_6]^{3-}$ units, whereas the shoulders at 2160 and 2162 cm^{-1}, respectively, are assigned to bridging CN^- ligands. Taking into account the Mössbauer data, we assign the stretching bands with lower frequency in **1** (2051 cm^{-1}) and **3** (2064 cm^{-1}) to the terminal CN^- ligands at Fe^{II} ions. The shoulder at 2110 cm^{-1} in the spectrum of **1** is attributed to the bridging CN^- ligands of Fe^{II}–C≡N–$Co_3(dpa)_4$ fragments. The spectrum of **3** is somewhat different, because it contains not just a shoulder to the high-energy side of 2064 cm^{-1} but also a band, the structure of which is similar to that of the C≡N stretching band observed in the spectrum of **4** (Figure 2). Yet again using the results of Mössbauer spectroscopy, which revealed the coexistence of comparable amounts of LS Fe^{II} and LS Fe^{III} ions in **3**, we attribute the high-energy feature in the IR spectrum of this complex to the terminal CN^- ligands at the Fe^{III} ions (2116 cm^{-1}) and to the bridging CN^- ligands of Fe^{III}–C≡N–$Co_3(dpa)_4$ fragments (2146 cm^{-1}). We also expect that the C≡N stretching band for the Fe^{II}–C≡N–$Co_3(dpa)_4$ fragments should be observed as a higher-energy shoulder of the 2064 cm^{-1} band, but it is masked by the band at 2116 cm^{-1}.

Electron Transfer

The IR and Mössbauer spectra of **1** and **3** conclusively establish the presence of LS Fe^{II} ions, which is the result of a complete or partial electron transfer taking place during the synthesis. It appears that **1** predominantly contains LS Fe^{II} ions, whereas **3** contains a mixture of LS Fe^{II} and LS Fe^{III} ions, the ratio of which is temperature-dependent.

To understand these results, we examined the redox properties of the precursors used for the preparation of **1**–**4**. The processes of interest in the present context are the oxidation of $M_3(dpa)_4Cl_2$ and the reduction of $[M'(CN)_6]^{3-}$. The formal potentials for the corresponding half-reactions are shown in Table 4. It is obvious that $[Co(CN)_6]^{3-}$ should be electrochemically inert with respect to both $Co_3(dpa)_4Cl_2$ and $Ni_3(dpa)_4Cl_2$. On the other hand, the half-wave potential $E_{1/2}$ of the $[Fe(CN)_6]^{3-}/[Fe(CN)_6]^{4-}$ couple, which is higher than that of the $Co_3(dpa)_4Cl_2^+/Co_3(dpa)_4Cl_2$ couple, indicates that $[Fe(CN)_6]^{3-}$ can oxidize $Co_3(dpa)_4Cl_2$. In the case of $Ni_3(dpa)_4Cl_2$, however, the oxidation by $[Fe(CN)_6]^{3-}$ is not feasible, although the $E_{1/2}$ values of the corresponding redox couples are quite close.

Table 4. $E_{1/2}$ values for half-reactions involving $M_3(dpa)_4Cl_2$ (M = Co, Ni) and $[M'(CN)_6]^{3-}$ (M′ = Fe, Co).

Redox couple	$E_{1/2}$ [V] (vs Fc^+/Fc)	Reference
$Co_3(dpa)_4Cl_2^+/Co_3(dpa)_4Cl_2$	0.32	[52]
$Ni_3(dpa)_4Cl_2^+/Ni_3(dpa)_4Cl_2$	0.49	[53]
$[Fe(CN)_6]^{3-}/[Fe(CN)_6]^{4-}$	0.41	this work
$[Co(CN)_6]^{3-}/[Co(CN)_6]^{4-}$	–1.45	this work

Of course, the relative redox potentials will be influenced by the formation of the CN-bridged structure, but we do not expect these changes to be very dramatic. In fact, the above analysis is in accord with the results of Mössbauer spectroscopy. The LS Fe^{II} centers prevail in sample **1**, which points to a complete electron transfer from $Co_3(dpa)_4Cl_2$ to $[Fe(CN)_6]^{3-}$ upon the formation of this complex. Because

the Co_3/Fe ratio in the elemental-analysis formula of **1** is approximately 2:1 (Table 1), the oxidation state of about one half of the tricobalt units in **1** is described as $[Co^{III}Co^{II}_2(dpa)_4]^{3+}$, whereas the other half remains in the original $[Co^{II}_3(dpa)]^{2+}$ state. A small amount of LS Fe^{III} ions was also observed in the Mössbauer spectrum of **1** (Table 2), which can be due to either the existence of trapped states or the presence of a minor impurity.

Sample **3** is a mixed-valent system that exhibits an equilibrium between the LS Fe^{II} and LS Fe^{III} ions, which thus suggests a partial charge transfer between the $[Ni_3(dpa)_4]^{2+}$ and $[Fe(CN)_6]^{3-}$ fragments. The Fe^{III}/Fe^{II} ratio increases for lower temperatures, which indicates that the Fe^{III}-containing configuration is the ground state of the system. This is in agreement with the analysis of electrochemical data that showed the oxidation of $Ni_3(dpa)_4Cl_2$ by $[Fe(CN)_6]^{3-}$ to be unlikely. Nevertheless, the energetic proximity of the $[Ni_3(dpa)_4]^{3+}/[Fe(CN)_6]^{4-}$ configuration to the $[Ni_3(dpa)_4]^{2+}/[Fe(CN)_6]^{3-}$ ground state results in the progressive population of the former as the temperature is increased. Indeed, at 295 K the Fe^{III}/Fe^{II} ratio already approaches 1 (Table 2).

XANES Spectroscopy

The Mössbauer spectroscopy results convincingly demonstrate the mixed valence of Fe in **3**. Unfortunately, this method is not readily available for the study of the oxidation state of Ni. To corroborate the partial charge transfer from $[Ni_3(dpa)_4]^{2+}$ to $[Fe(CN)_6]^{3-}$, we turned to X-ray absorption near edge structure (XANES) spectroscopy, which has been used as an effective tool for the determination of the oxidation state of various metal ions.[54–56]

The room-temperature Ni *K*-edge XANES spectra of **3** and **4** reveal several contributions to the absorption threshold that are resolved completely or partially (Figure 3a). The strong contribution A is due to the main dipole 1s→4p electron transition. The features B1 and B2 are due to the 1s→4s transition, which is probably split by the crystal field. The weak pre-edge features C1 and C2 are caused by the dipole-forbidden crystal-field transition from the core 1s level to the empty states of the 3d level, which is possibly 4p-hybridized by the ligands.[57,58]

The shifts of main XANES contributions to higher energies can indicate an increase in the oxidation state of the Ni ions. On the basis of the foregoing discussion of electrochemical, IR, and Mössbauer data, compound **4** should contain Ni ions only in the +2 state, whereas the average oxidation state of Ni in **3** should increase because of the partial charge transfer from $[Ni_3(dpa)_4]^{2+}$ to $[Fe(CN)_6]^{3-}$. One can estimate, however, that even at room temperature, when the degree of charge transfer and the concentration of Fe^{II} centers are the highest, the average oxidation state of Ni should not exceed +2.09. Such a small difference will hardly be resolved in the Ni *K*-edge XANES spectra because of various peak-broadening mechanisms. The second derivative of the experimental spectra (Figure 3b) allows a more accurate estimation of the peak positions.[57] Our analysis reveals that all XANES contributions experience positive shifts upon going from sample **4** to sample **3** (Table S1). This points to a total positive shift of the entire absorption threshold and to a corresponding increase in the average oxidation state of Ni.

The values of the spectral shifts, however, are extremely small (and so is the expected change in the average oxidation state) and actually beyond the accuracy of the method employed. Therefore, we also evaluated the Ni oxidation state by analyzing the pre-edge features C1 and C2, which are located around 8333 eV (Figure 3a). The intensity of these dipole-forbidden features is approximately 30–35 times lower than the absorption-edge intensity, but the position, shape, and number of pre-edge peaks are very sensitive to the oxidation state and coordination environment of the 3d-metal ion.[57,58] The pre-edge region is much less influenced by medium- and long-range crystal-structure effects, which makes it more attractive for the accurate estimation of oxidation states than the second derivative of the experimental spectra.

The pre-edge features of samples **3** and **4** (Figure 4) were extracted by means of a XANES-pre-edge analysis proposed in the literature.[58] They consist of two contributions, C1 and C2 (a third, small feature at 8336 eV is due to the imperfection of the pre-edge extraction). The position of C1 is the same for both samples, but C2 is shifted to slightly higher energies in the spectrum of **3** relative to its position in the spectrum of **4** (by ca. 0.15 eV). This shift might indicate the slight increase in the Ni oxidation state.

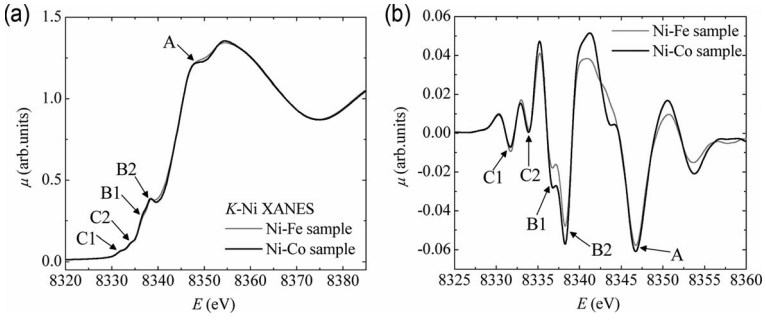

Figure 3. Ni *K*-edge XANES spectra of **3** and **4** (a) and their second derivatives (b). The main spectral contributions are marked.

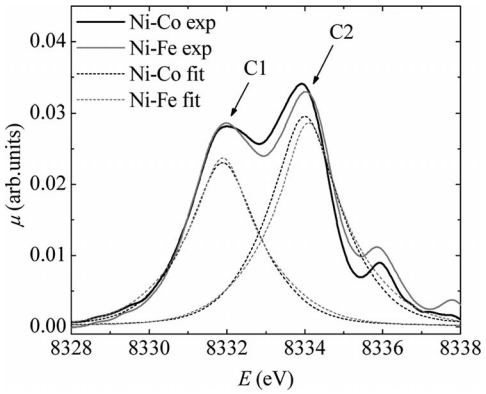

Figure 4. Pre-edge features extracted from XANES spectra of **3** and **4**. The fitting functions for C1 and C2 contributions are also shown to clearly demonstrate the slight shift of the pre-edge in **3** relative to that in **4**.

Although XANES data suggest a slight increase in the average oxidation state of Ni in sample **3** relative to sample **4**, the exact value of this increase cannot be obtained, because a sample solely containing Ni^{3+} ions in a similar coordination environment is unavailable. Besides, the extracted shifts of main XANES contributions and the pre-peak centroid (Figure S2) in the spectrum of **3** in comparison to the spectrum of **4** are extremely small. Therefore, the XANES spectroscopy results confirm a small increase in the Ni oxidation state, which is in accord with the analysis of Mössbauer data.

Magnetic Properties

We first present and discuss the magnetic behavior of **2** and **4**, which can be considered as model compounds for **1** and **3**, respectively, because they contain diamagnetic $[Co^{III}(CN)_6]^{3-}$ fragments and do not exhibit changes in the oxidation state of $[M_3(dpa)_4]^{2+}$ units as compared to the starting materials.

At 300 K, the χT value of **2** is 3.74 emu K mol^{-1}, which can be normalized to 1.82 emu K mol^{-1} per $[Co_3(dpa)_4]^{2+}$ unit. The latter value falls in the range of χT values reported for symmetric (1.28 emu K mol^{-1}) and unsymmetric (2.47 emu K mol^{-1}) forms of the $Co_3(dpa)_4Cl_2$ starting material.[37] Therefore, it can be assumed that both forms of the tricobalt unit are present in the structure of **2**, which is not at all unexpected, given the amorphous, disordered nature of this material. The temperature dependence of χT for **2** essentially follows that of its precursor complex and exhibits a gradual decrease as the temperature is lowered (Figure 5a). This decrease is associated with the well-established spin crossover of the tricobalt cluster, which is due to the depopulation of the S = 5/2 and S = 3/2 states in favor of the S = 1/2 ground state of $[Co_3(dpa)_4]^{2+}$. The field-dependent magnetization measured at 1.8 K exhibits the maximum value of 2.53 μ_B, or 1.23 μ_B per $[Co_3(dpa)_4]^{2+}$ unit, at 7 T (Figure 6), which is in good agreement with the saturation magnetization of 1.20 μ_B reported for $Co_3(dpa)_4Cl_2$.[37]

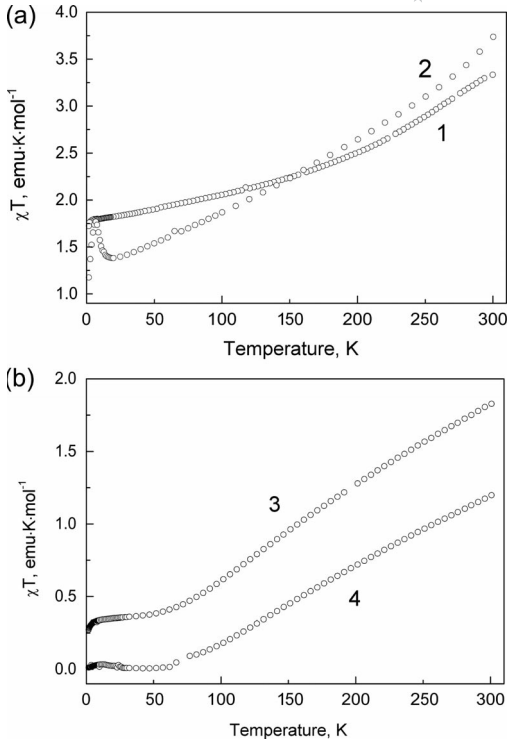

Figure 5. Temperature dependences of χT for **1** and **2** (a) and **3** and **4** (b) measured in an applied magnetic field of 0.1 T.

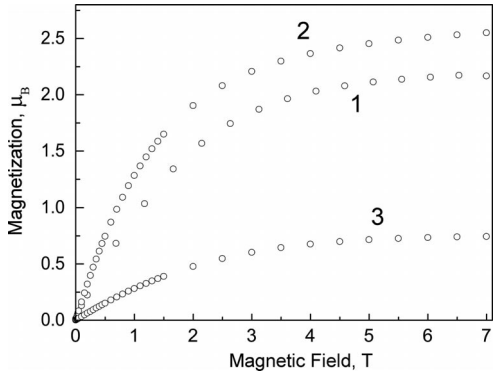

Figure 6. Field-dependent magnetization of **1**, **2**, and **3** measured at 1.8 K.

Nevertheless, unlike $Co_3(dpa)_4Cl_2$, sample **2** exhibits an abrupt increase of χT at lower temperatures. Temperature-dependent magnetization measurements performed in zero-field-cooled (ZFC) and field-cooled (FC) modes showed a divergence between the ZFC and FC magnetization curves at 4.8 K (Figure 7). Consequently, the alternating-current (AC) susceptibility was examined around this temperature, and this revealed frequency-dependent peaks in the real and imaginary parts of the susceptibility (Figure 7, inset). The empirical Mydosh parameter was calculated as $\phi = (T_{max}{}^{vi} - T_{max}{}^{v2})/[T_{max}{}^{vi}(\log \nu_i - \log \nu_2)]$, where $T_{max}{}^{vi}$ is the temperature of the maximum in the χ' vs. T curve at the corresponding frequency. The obtained value of ϕ = 0.052(2) is in the range typical for spin glasses (0.004–0.08).[59] The spin-glass transition arises from the magnetic

superexchange coupling between the $[Co_3(dpa)_4]^{2+}$ units, which is mediated by the diamagnetic $[Co(CN)_6]^{3-}$ bridges. Such coupling was also proposed to operate in other assemblies with diamagnetic hexacyanometalate linkers[11,60] and was confirmed by experimental evidences.[61]

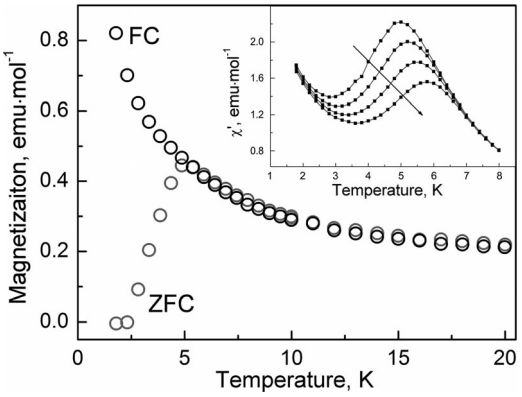

Figure 7. Temperature dependence of field-cooled (FC, black) and zero-field-cooled (ZFC, gray) magnetizations of **2** measured with an applied field of 0.0005 T. Inset: Temperature dependence of the real part of the AC magnetic susceptibility at various frequencies of the applied AC field.

Sample **4** exhibits a 300 K χT value of 1.20 emu K mol^{-1}. Normalizing this value gives approximately 0.76 emu K mol^{-1} per $[Ni_3(dpa)_4]^{2+}$ unit, which is in good agreement with the value of 0.75 emu K mol^{-1} reported for $Ni_3(dpa)_4(dca)_2$ (dca = dicyanamide), a complex with a similar coordination environment around the trinickel unit.[62] Similar to the latter, the χT value of **4** gradually decreases as the temperature is lowered and becomes close to zero below 60 K (Figure 5b), owing to the essentially complete population of the diamagnetic ground state.

The 300 K χT value for sample **1** is 3.33 emu K mol^{-1}, or 1.69 emu K mol^{-1} per $[Co_3(dpa)_4]^{2+}$ unit, which is slightly lower than the value observed for sample **2** (1.82 emu K mol^{-1}). If no electron transfer between $[Co_3(dpa)_4]^{2+}$ and $[Fe(CN)_6]^{3-}$ ions took place during the synthesis, the χT value of **1** should increase relative to that of **2**. The electron transfer, however, not only results in diamagnetic Fe^{II} centers, but it is also expected to lower the spin state of the oxidized trimetallic units. Indeed, $[Co_3(dpa)_4Cl_2](BF_4)$ exhibited a lower χT value (0.91 emu K mol^{-1} at 300 K)[52] than $Co_3(dpa)_4Cl_2$ (> 1.28 emu K mol^{-1}). Therefore, the decrease in the χT value upon going from **2** to **1** is in agreement with the electron-transfer event established on the basis of Mössbauer and IR data. The χT value of **1** gradually decreases with the temperature but remains quite large below 100 K, and even higher than the χT value of **2** (Figure 5a). The maximum magnetization value attained at 1.8 K and 7 T is 2.19 μ_B, or 1.11 μ_B per $[Co_3(dpa)_4]^{2+}$ unit, which is slightly lower than the value obtained for sample **2**, yet again in accord with the presence of diamagnetic Fe^{II} ions and oxidized $[Co_3(dpa)_4]^{3+}$ units in sample **1**.

The χT value of **3** at 300 K is 1.83 emu K mol^{-1}, or 1.05 emuK mol^{-1} per $[Ni_3(dpa)_4]^{2+}$ unit, and the χT curve remains higher than that of **4** in the entire temperature range (Figure 5b). This agrees with the presence of paramagnetic LS Fe^{III} ions in the sample. Below 50 K, the χT value reaches a plateau of approximately 0.35 emu K mol^{-1} per formula unit, which is close to the value of 0.375 emu K mol^{-1} expected for a single $S = 1/2$ center. The saturation-magnetization value of 0.74 μ_B per formula unit at 1.8 K and 7 T is slightly lower than expected for $S = 1/2$, which might be explained by the anisotropy of the g-factor.

Conclusions

This study demonstrates that the trimetallic complexes $M_3(dpa)_4Cl_2$ (M = Co, Ni) are useful building blocks for the construction of CN-bridged coordination frameworks. To the best of our knowledge, compounds **1**–**4** represent the first examples of coordination polymers incorporating the $[M_3(dpa)_4]^{2+}$ units. The latter act as ditopic linkers connecting the $[M'(CN)_6]^{3-}$ anions (M′ = Fe, Co) to form an extended 2D structure. The bulkiness of the dpa^- ligands that surround the trimetallic core in $[M_3(dpa)_4]^{2+}$ precludes the formation of a 3D structure with PB topology. The unique properties of the trimetallic clusters translate into an interesting electronic and magnetic behavior of the obtained extended structures. The combination of IR and Mössbauer spectroscopy in conjunction with the analysis of the redox behavior of the employed building blocks indicates the oxidation of $[Co_3(dpa)_4]^{2+}$ ions by $[Fe(CN)_6]^{3-}$ ions and a partial charge transfer between $[Ni_3(dpa)_4]^{2+}$ and $[Fe(CN)_6]^{3-}$ ions upon the formation of the corresponding frameworks. These findings incite us to further explore the chemistry of trimetallic building blocks, which can have implications for the preparation of coordination polymers capable of exhibiting temperature- and light-induced spin transitions. Efforts in this direction are currently under way in our laboratories.

Experimental Section

Synthesis: All reactions were performed under N_2 by using standard Schlenk techniques, unless noted otherwise. All reagents were purchased from Aldrich and used as received. $Co_3(dpa)_4Cl_2$[45] and $Ni(Hdpa)Cl_2$[44] were synthesized according to the published procedures. The compounds $(Bu_4N)_3[M'(CN)_6]$ (M′ = Fe, Co) were prepared by mixing an aqueous solution of the corresponding potassium salt (5 M) with an aqueous solution of $(Bu_4N)Cl$ (2 M) and recrystallizing the obtained precipitate from CH_2Cl_2/hexanes. Anhydrous, commercial solvents were additionally purified by passing through a double-stage drying/purification system (Glass Contour Inc.).

$Ni_3(dpa)_4Cl_2 \cdot 1.2CH_2Cl_2$: To a mixture of $Ni(Hdpa)Cl_2$ (0.903 g, 3.00 mmol) and Hdpa (0.171 g, 1.00 mmol) in a Schlenk flask (100 mL) was added anhydrous THF (30 mL). After the obtained suspension was cooled to –78 °C in a dry ice/acetone bath, a solution of methyllithium in diethyl ether (4.0 mmol, 2.5 mL, 1.6 M) was added dropwise. The color turned to yellow-brown. The mixture was warmed up to room temperature, at which point the color

changed to a dark, reddish brown. The mixture was heated to reflux under N_2 flow overnight, which resulted in a dark-purple suspension. After cooling down to room temperature, the solvent was evaporated to dryness under reduced pressure. The obtained solid residue was extracted with dichloromethane (30 mL) to give a dark-purple solution, onto which was carefully layered hexanes (50 mL). Large purple-red needle-like crystals were obtained after 1 week. Yield 84.3% (0.868 g). $C_{41.2}H_{24.4}Cl_{4.4}N_{12}Ni_3$ [$Ni_3(dpa)_4 \cdot 1.2CH_2Cl_2$]: calcd. C 48.06, H 3.37, Cl 15.15, N 16.32; found C 48.41, H 3.27, Cl 15.06, N 16.18.

{[$Co_3(dpa)_4$]$_{1.97}$[$Fe(CN)_6$]}$Cl_{0.8}$ (1): A solution of $(Bu_4N)_3[Fe(CN)_6]$ (0.042 g, 0.045 mmol) in DMF (10 mL) was added dropwise to a solution of $Co_3(dpa)_4Cl_2$ (0.148 g, 0.135 mmol) in DMF (10 mL) with vigorous stirring. A dark-brown precipitate formed quickly. After stirring the mixture at room temperature for 1 h, the precipitate was recovered by filtration, washed consecutively with DMF (3 × 15 mL), and dried under vacuum. Yield 0.062 g. $C_{84.8}H_{88.2}Cl_{0.8}Co_{5.9}FeN_{29.6}O_{12.6}$ (**1**·12.6H_2O): calcd. C 47.23, H 4.12, Cl 1.32, N 19.25; found C 47.33, H 3.77, Cl 1.26, N 18.89.

{[$Co_3(dpa)_4$]$_{2.06}$[$Co(CN)_6$]}$Cl_{1.1}$ (2), {[$Ni_3(dpa)_4$]$_{1.74}$[$Fe(CN)_6$]}$Cl_{0.45}$ (3), and {[$Ni_3(dpa)_4$]$_{1.57}$[$Co(CN)_6$]}$Cl_{0.3}$ (4) were obtained as dark-brown, dark-purple, and dark-purple precipitates, respectively, in a manner analogous to that described for **1** above. $C_{88.4}H_{88.5}Cl_{1.1}Co_{7.2}N_{30.7}O_{11.3}$ (**2**·11.3H_2O): calcd. C 47.76, H 4.01, Cl 1.75, N 19.35; found C 47.74, H 3.52, Cl 2.08, N 18.87. $C_{75.6}H_{67.9}Cl_{0.45}FeN_{26.9}Ni_{5.2}O_{6.1}$ (**3**·6.1H_2O): calcd. C 49.68, H 3.74, Cl 0.87, N 20.60; found C 49.85, H 3.72, Cl 0.69, N 20.73. $C_{68.8}H_{62.0}Cl_{0.3}CoN_{24.8}Ni_{4.7}O_{5.9}$ (**4**·5.9H_2O): calcd. C 49.27, H 3.73, Cl 0.63, N 20.74; found C 49.14, H 3.58, Cl 0.56, N 20.66.

Magnetic Measurements: Magnetic measurements were performed on powder samples with a Quantum Design SQUID magnetometer MPMS-XL. DC magnetic susceptibility measurements were carried out with an applied field of 0.1 T in the temperature range 1.8–300 K. Isothermal dependences of the magnetization were measured at 1.8 K in the field range 0–7 T. The AC magnetic susceptibility was measured under zero DC-bias field in the range 1.8–50 K, with an AC-field amplitude of 0.0003 T and frequencies of 1, 10, 100, and 1000 Hz.

Mössbauer Spectroscopy: Mössbauer spectra were acquired by using a conventional constant-acceleration spectrometer operated in a multi-channel scaling mode. The γ-ray source consisted of approximately 60 mCi of ^{57}Co in a rhodium matrix that was maintained at ambient temperature. The pulse-height-analysis spectrum for the ^{57}Co/Rh 14.4 keV γ-ray source was determined by using a Reuter–Stokes gas proportional counter filled to 1 atm with a Kr/CO_2 gas mixture. The isomer shifts were determined relative to the center of an Fe-foil absorber.

Infrared Spectroscopy: IR spectra were measured in the range 600–4000 cm^{-1} with solid samples pressed on a zinc selenide crystal of the universal attenuated-total-reflectance (ATR) sampling accessory of a Perkin–Elmer Spectrum 100 FT-IR spectrometer.

Diffuse Reflectance Spectroscopy: The diffuse reflectance data were collected with a Perkin–Elmer-Lambda 900 UV/Vis/NIR spectrophotometer equipped with a 160 mm integrating sphere. The spectra were measured as total reflectance spectra and converted to Kubelka–Munk units (Figure S1).

Electrochemistry: Cyclic voltammograms (CV) were recorded with a CH Instruments 600D electrochemical analyzer by using a Pt-disc working electrode, a Pt-wire auxiliary electrode, and an Ag/Ag^+ reference electrode containing $AgNO_3$ (0.01 M) and Bu_4NPF_6 (0.1 M) in acetonitrile. CV measurements were performed at room temperature under N_2 with a solution of Bu_4NPF_6 (0.1 M) in DMF as supporting electrolyte at a sweep rate of 0.1 $V s^{-1}$. All measured potentials were referenced to the Fc^+/Fc couple (Fc = ferrocene), which was added as an internal standard upon completion of each experiment.

XANES Spectroscopy: The X-ray absorption near edge structure (XANES) spectra were collected at C beamline of DORIS-III storage ring (HASYLAB/DESY, Hamburg, Germany). The spectra were acquired at the *K*-Ni absorption edge (8333 eV) in transmission mode at room temperature. A double-crystal Si(311) monochromator with an energy resolution of approximately 8.5×10^{-5} dEE^{-1} (ca. 0.7 eV at 8333 eV) was used.

Supporting Information (see footnote on the first page of this article): Diffuse reflectance spectra, detailed analysis of XANES spectra.

Acknowledgments

M. S. gratefully acknowledges the National Science Foundation (NSF) for the support of this research (grant CHE-0911109). The Mössbauer spectra were taken at the National High Magnetic Field Laboratory (NHMFL), which is funded by the NSF through the Cooperative Agreement DMR-0654118, the State of Florida, and the Department of Energy. The Mössbauer instrument was purchased by using the User Collaboration Grant Program UCGP 5064 funds awarded to A. O. We thank Dr. Adrian Lita (Florida State University) for assistance with the acquisition of diffuse-reflectance spectra and Dr. Robert Goddard (NHMFL) for assistance with the EDX analysis.

[1] S. Ferlay, T. Mallah, R. Ouahes, P. Veillet, M. Verdaguer, *Nature* **1995**, *378*, 701.
[2] W. R. Entley, G. S. Girolami, *Science* **1995**, *268*, 397.
[3] S. M. Holmes, G. S. Girolami, *J. Am. Chem. Soc.* **1999**, *121*, 5593.
[4] O. Sato, T. Iyoda, A. Fujishima, K. Hashimoto, *Science* **1996**, *272*, 704.
[5] H. Tokoro, S. Ohkoshi, *Dalton Trans.* **2011**, *40*, 6825.
[6] K. W. Chapman, P. D. Southon, C. L. Weeks, C. J. Kepert, *Chem. Commun.* **2005**, 3322.
[7] S. S. Kaye, J. R. Long, *J. Am. Chem. Soc.* **2005**, *127*, 6506.
[8] S. Margadonna, K. Prassides, A. N. Fitch, *J. Am. Chem. Soc.* **2004**, *126*, 15390.
[9] A. L. Goodwin, K. W. Chapman, C. J. Kepert, *J. Am. Chem. Soc.* **2005**, *127*, 17980.
[10] K. W. Chapman, P. J. Chupas, C. J. Kepert, *J. Am. Chem. Soc.* **2006**, *128*, 7009.
[11] M. Shatruk, C. Avendano, K. R. Dunbar, *Prog. Inorg. Chem.* **2009**, *56*, 155.
[12] R. Lescouezec, L. M. Toma, J. Vaissermann, M. Verdaguer, F. S. Delgado, C. Ruiz-Perez, F. Lloret, M. Julve, *Coord. Chem. Rev.* **2005**, *249*, 2691.
[13] M. Ferbinteanu, H. Miyasaka, W. Wernsdorfer, K. Nakata, K. i. Sugiura, M. Yamashita, C. Coulon, R. Clerac, *J. Am. Chem. Soc.* **2005**, *127*, 3090.
[14] T. Liu, Y. J. Zhang, S. Kanegawa, O. Sato, *J. Am. Chem. Soc.* **2010**, *132*, 8250.
[15] J. N. Rebilly, T. Mallah, *Struct. Bonding (Berlin)* **2006**, *122*, 103.
[16] K. Mitsumoto, E. Oshiro, H. Nishikawa, T. Shiga, Y. Yamamura, K. Saito, H. Oshio, *Chem. Eur. J.* **2011**, *17*, 9612 .
[17] S. Wang, X. H. Ding, J. L. Zuo, X. Z. You, W. Huang, *Coord. Chem. Rev.* **2011**, *255*, 1713.
[18] J. J. Sokol, A. G. Hee, J. R. Long, *J. Am. Chem. Soc.* **2002**, *124*, 7656.

[19] E. J. Schelter, A. V. Prosvirin, K. R. Dunbar, *J. Am. Chem. Soc.* **2004**, *126*, 15004.
[20] C. P. Berlinguette, D. Vaughn, C. Canada-Vilalta, J. R. Galan-Mascaros, K. R. Dunbar, *Angew. Chem.* **2003**, *115*, 1561; *Angew. Chem. Int. Ed.* **2003**, *42*, 1523.
[21] J. Lu, W. T. A. Harrison, A. J. Jacobson, *Chem. Commun.* **1996**, 399.
[22] D. Yoshioka, M. Mikuriya, M. Handa, *Chem. Lett.* **2002**, 1044.
[23] T. E. Vos, Y. Liao, W. W. Shum, J. H. Her, P. W. Stephens, W. M. Reiff, J. S. Miller, *J. Am. Chem. Soc.* **2004**, *126*, 11630.
[24] B. S. Kennon, K. H. Stone, P. W. Stephens, J. S. Miller, *CrystEngComm* **2009**, *11*, 2185.
[25] S. Jin, F. J. DiSalvo, *Chem. Mater.* **2002**, *14*, 3448.
[26] B. Yan, H. Zhou, A. Lachgar, *Inorg. Chem.* **2003**, *42*, 8818.
[27] N. G. Naumov, A. V. Virovets, S. B. Artemkina, D. Y. Naumov, J. A. K. Howard, V. E. Fedorov, *J. Solid State Chem.* **2004**, *177*, 1896.
[28] J. F. Berry, "Extended metal atom chains" in *Multiple Bonds Between Metal Atoms*, 3rd ed. (Eds.: F. A. Cotton, C. A. Murillo, R. A. Walton), Springer, New York, **2005**, pp. 669–706.
[29] E. C. Yang, M. C. Cheng, M. S. Tsai, S. M. Peng, *J. Chem. Soc., Chem. Commun.* **1994**, 2377.
[30] F. A. Cotton, L. M. Daniels, C. A. Murillo, I. Pascual, *J. Am. Chem. Soc.* **1997**, *119*, 10223.
[31] R. Clerac, F. A. Cotton, K. R. Dunbar, C. A. Murillo, I. Pascual, X. Wang, *Inorg. Chem.* **1999**, *38*, 2655.
[32] J. F. Berry, F. A. Cotton, T. Lu, C. A. Murillo, B. K. Roberts, X. Wang, *J. Am. Chem. Soc.* **2004**, *126*, 7082.
[33] C. K. Kuo, I. P.-C. Liu, C. Y. Yeh, C. H. Chou, T. B. Tsao, G. H. Lee, S. M. Peng, *Chem. Eur. J.* **2007**, *13*, 1442.
[34] J. F. Berry, F. A. Cotton, C. A. Murillo, *Inorg. Chim. Acta* **2004**, *357*, 3847.
[35] J. Wang, Z. Wang, R. J. Clark, A. Ozarowski, J. van Tol, N. S. Dalal, *Polyhedron* **2011**, *30*, 3058.
[36] R. Clerac, F. A. Cotton, L. M. Daniels, K. R. Dunbar, C. A. Murillo, X. Wang, *Inorg. Chem.* **2001**, *40*, 1256.
[37] R. Clerac, F. A. Cotton, L. M. Daniels, K. R. Dunbar, K. Kirschbaum, C. A. Murillo, A. A. Pinkerton, A. J. Schultz, X. Wang, *J. Am. Chem. Soc.* **2000**, *122*, 6226.
[38] We do not include in this consideration the direct extension of the trimetallic units with additional metal atoms, which results in penta-, hepta-, and even undecanuclear clusters. The rich chemistry of these linear metallic units has been reviewed in ref.[28]
[39] C. H. Peng, C. C. Wang, H. C. Lee, W. C. Lo, G. H. Lee, S. M. Peng, *J. Chin. Chem. Soc.* **2001**, *48*, 987.
[40] J. Zhang, L. G. Zhu, *CrystEngComm* **2011**, *13*, 553.
[41] T. B. Tsao, G. H. Lee, C. Y. Yeh, S. M. Peng, *Dalton Trans.* **2003**, 1465.
[42] L. G. Zhu, S. M. Peng, G. H. Lee, *Chem. Lett.* **2002**, 1210.
[43] J. F. Berry, F. A. Cotton, L. M. Daniels, C. A. Murillo, X. Wang, *Inorg. Chem.* **2003**, *42*, 2418.
[44] T. J. Hurley, M. A. Robinson, *Inorg. Chem.* **1968**, *7*, 33.
[45] F. A. Cotton, L. M. Daniels, G. T. Jordan, C. A. Murillo, *J. Am. Chem. Soc.* **1997**, *119*, 10377.
[46] K. R. Dunbar, R. A. Heintz, *Prog. Inorg. Chem.* **1997**, *45*, 283.
[47] V. Escax, A. Bleuzen, C. Cartier dit Moulin, F. Villain, A. Goujon, F. Varret, M. Verdaguer, *J. Am. Chem. Soc.* **2001**, *123*, 12536.
[48] N. Shimamoto, S. Ohkoshi, O. Sato, K. Hashimoto, *Inorg. Chem.* **2002**, *41*, 678.
[49] T. Matsuda, J. Kim, Y. Moritomo, *J. Am. Chem. Soc.* **2010**, *132*, 12206.
[50] J. Fernandez Bertran, E. Reguera-Ruiz, J. Blanco Pascual, *Spectrochim. Acta Part A* **1990**, *46A*, 1679.
[51] E. Reguera, J. Fernandez-Bertran, J. Balmaseda, *Trans. Met. Chem.* **1999**, *24*, 648.
[52] R. Clerac, F. A. Cotton, K. R. Dunbar, T. Lu, C. A. Murillo, X. Wang, *J. Am. Chem. Soc.* **2000**, *122*, 2272.
[53] J. F. Berry, F. A. Cotton, L. M. Daniels, C. A. Murillo, *J. Am. Chem. Soc.* **2002**, *124*, 3212.
[54] J. Röhler, *J. Magn. Magn. Mater.* **1975**, *47–48*, 175.
[55] A. Bianconi, S. Modesti, M. Campagna, K. Fisher, S. Stlzza, *J. Phys. C* **1981**, *14*, 4737.
[56] K. Kovnir, W. M. Reiff, A. P. Menushenkov, A. A. Yaroslavtsev, R. V. Chernikov, M. Shatruk, *Chem. Mater.* **2011**, *23*, 3021.
[57] G. Sankar, P. R. Sarode, C. N. R. Rao, *Chem. Phys.* **1983**, *76*, 435.
[58] E. Chalmin, F. Farges, G. E. Brown Jr., *Contrib. Mineral. Petrol.* **2009**, *157*, 111.
[59] J. A. Mydosh, *Spin Glasses – an Experimental Introduction*, Taylor & Francis, Washington, DC, **1993**.
[60] M. Shatruk, K. E. Chambers, A. V. Prosvirin, K. R. Dunbar, *Inorg. Chem.* **2007**, *46*, 5155.
[61] M. Shatruk, A. Dragulescu-Andrasi, K. E. Chambers, S. A. Stoian, E. L. Bominaar, C. Achim, K. R. Dunbar, *J. Am. Chem. Soc.* **2007**, *129*, 6104.
[62] J. F. Berry, F. A. Cotton, C. A. Murillo, *Dalton Trans.* **2003**, 3015.

Received: March 17, 2012
Published Online: July 16, 2012

